www.czasopisma.pan.pl PAN POLSKA AKADEMIA NAUK www.journals.pan.pl

A R C H I V E S O F M E T A L L U R G Y A N D M A T E R I A L S

Volume 58 2013 Issue 3

DOI: 10.2478/amm-2013-0060

Z. PATER*, J. KAZANECKI**

COMPLEX NUMERICAL ANALYSIS OF THE TUBE FORMING PROCESS USING DIESCHER MILL

KOMPLEKSOWA ANALIZA NUMERYCZNA PROCESU WALCOWANIA TULEI W WALCARCE DIESCHERA

This paper presents the results of FEM simulations of the rotary piercing process in which disc guiding devices of the Diescher type are used. During this process the material is formed by means of two skew rolls, two guiding devices, and the piercing plug mounted on the mandrel. The aim of the analysis was to determine the effect of the plug diameter, the plug advance, the feed angle and the diameter reduction on the piercing process. Nine cases of piercing with three different plugs used were analyzed. The effects of the basic process parameters on the tube shell diameter and the tool load were analyzed. The numerical results obtained using Simufact.Forming 10.0 were verified under experimental conditions in which the tube shell made from 100Cr6 bearing steel was pierced. The results of the FEM calculations show agreement with the experimental results.

Keywords: tube piercing, Diescher mill, FEM analysis, experiment

W artykule zaprezentowano wyniki symulacji numerycznych procesu dziurowania tulei w walcarce skośnej z prowadnicami tarczowymi Dieschera. W procesie tym materiał jest kształtowany w wyniku oddziaływania dwóch ustawionych skośnie walców, dwóch prowadnic oraz główki dziurującej montowanej na trzpieniu. Celem analizy było określenie wpływu średnicy główki, wysunięcia główki, kąta zukosowania walców oraz gniotu na przebieg procesu dziurowania. Przeanalizowano dziewięć przypadków kształtowania, w których wykorzystano trzy rożne główki dziurujące. Określono wpływ podstawowych parametrów procesu na średnicę tulei kształtowanej oraz obciążenie poszczególnych narzędzi. Wyniki symulacji numerycznej otrzymanej w programie Simufact.Forming 10 zweryfikowano w warunkach doświadczalnych, w których dziurowano tuleje ze stali łożyskowej w gatunku 100Cr6. Rezultaty obliczeń MES pozostawały w dobrej zgodności z wynikami uzyskanymi z doświadczeń.

1. Introduction

Skew piercing mills are used to produce thick-walled tube shells which are then used to produce seamless pipes. Depending on the number of rolls, the skew mills can be divided into:

- two-roll mills with two working rolls and two guiding devices which hold the tube shell along the rolling axis. Such guiding devices may either be roll guides of the Mannesmann type, flat guides of the Stiefel type, or disc guides of the Diescher type;
- three-roll mills with three working rolls which operate without any additional guiding devices for the metal.

Out of the machines enumerated above, the two-roll mills equipped with the conical rolls and with the disc guiding devices of the Diescher type have the highest production capacity and guarantee the highest product accuracy [1].

Despite its over a hundred-year-old history of industrial applications, the rotary piercing process has not been satisfactorily researched yet, which can be attributed to very complex material flow kinematics. Nevertheless, an intensive development of numerical modelling methods for volumetric metal forming processes offers possibilities of improving the current state of knowledge about the process.

The first studies on numerical modelling of rotary piercing conducted in the last decade of the twentieth century were based on two-dimensional FEM models. For instance, Urbanski et al. [2] assumed an axially-symmetric shape of the semi-finished product, omitting, at the same time, the circumferential material flow, and thereby they were able to determine strain and temperature distributions in the longitudinal section of the semi-finished product. Due to the complex material flow, piercing processes should be modelled in three-dimensional state of strain conditions. Pietsch and Thievien [3], Ceretti et al. [4], and Komori [5] were the first to perform the three-dimensional modelling of the piercing process. However, the numerical models developed by the mentioned authors were based on significant simplifications – for instance, thermal phenomena occurring in the material were omitted, the calculations were limited only to the initial or steady state of the piercing process, or they assumed that the material being formed is ideally plastic. More developed models of the piercing process which took the thermal phenomena

* LUBLIN UNIVERSITY OF TECHNOLOGY, LUBLIN, POLAND

** AGH UNIVERSITY OF SCIENCE AND TECHNOLOGY, AL. A. MICKIEWICZA 30, 30-059 KRAKÓW, POLAND

into consideration were presented by Pater et al. [6] and Lu et al. [7]. The calculation results obtained by means of such models agree with the experimental test results. However, one shortcoming of these works is that the analysis was limited only to a single piercing case.

Pater and Kazanecki [8] presented the results of a piercing process simulation in which they applied the finite element method and focused on the analysis of state of stress and temperature distributions in the piercing plug. As a result of the calculations made, they determined that the highest thrusts (approx. 100-180 MPa) occur on the plug nose where the temperature quickly rises to exceed 900°C. It should also be mentioned that there were several other studies undertaken to investigate the piercing process. For example, Komori and Mizumo [9] used physical modelling (and deformed clay specimens) to determine the effect of the basic parameters on the course of piercing by means of the conical rolls. Ghiotti et al. [10] used the Forge software to model the barrel-type rotary piercing process (without the use of the piercing plug) and thus to determine the moment in which material cracking occurs in the product being formed. Pschera et al. [11] examined the effect of the feed angle of the rolls on material cracking in the pierced tube shell. Romanenko et al. [12] used infrared mapping to investigate temperature changes in the semi-finished product during the piercing process.

Summing up the literature overview, it can be observed that despite a number of works on modelling the rotary tube piercing process, there is still a need for a complex study which would analyze the effect of the basic process parameters on the course of the process. The present authors have undertaken to provide such study, and the present paper will discuss the numerical simulation results of several cases of the piercing process performed using the Diescher mill.

2. Applied model of piercing process and calculation scope

The numerical analysis of the piercing process was conducted using Simufact.Forming 10.0 which uses the FEM displacement representation [13, 14]. In the calculations nine cases of tube piercing in the two-roll skew mill with the disc guiding devices of the Diescher type were analyzed. A scheme of one of the analyzed cases is shown in Fig. 1, where the basic geometric parameters are also indicated. The following are changed in the calculations: the plug diameter d_g and its axial position c, the feed angle α, the roll spacing a and the disc spacing b. The change in the roll spacing results in the change in the reduction δ of the external diameter of the tube shell, which is determined as:

$$\delta = \frac{d_0 - d_{min}}{d_0} 100\% \tag{1}$$

where d_0 denotes the billet diameter, d_{min} denotes the minimal diameter of the necking formed on the tube shell (equal to the difference between the roll spacing a and the roll diameter d_R; $d_{min} = a\text{-}d_R$).

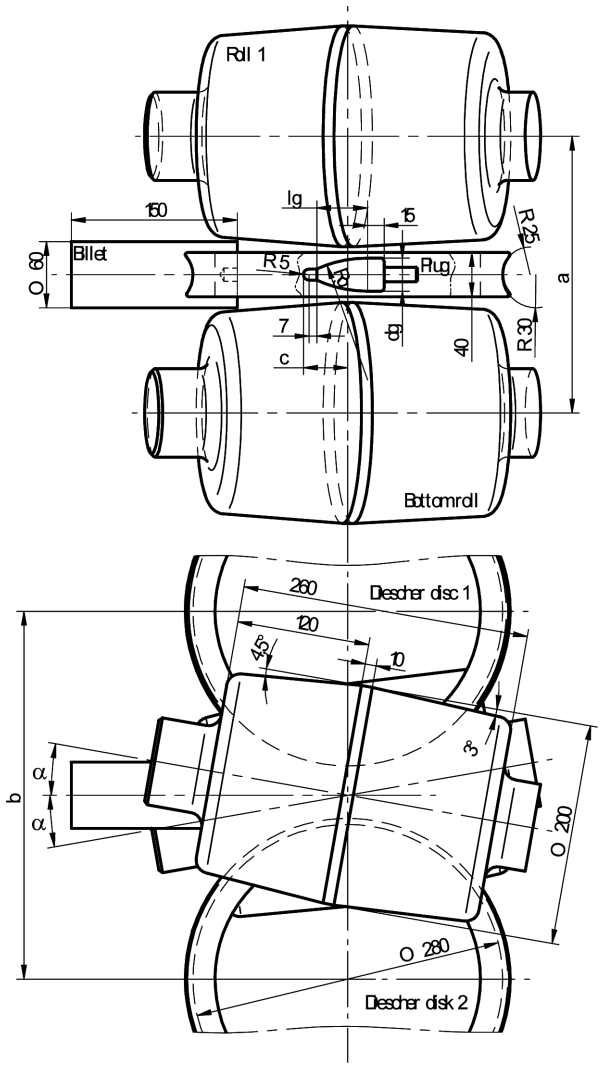

Fig. 1. Scheme of the analyzed rotary piercing process, with the most important parameters indicated

A detailed comparison of the variable parameters assumed in specific cases is shown in Table 1. It was assumed that the billet is in the form of a cylindrical specimen (with the diameter dimensions of 60 mm by 150 mm) made from steel grade 100Cr6, whose material model was taken from the material model database of the software used. The following are assumed: the rolls rotate in the same direction with a constant rotational velocity of n=60 turns/min, the discs rotate (in the opposite directions) with a velocity of 6.8 turns/min, and the plug is put into motion by the semi-product being formed.

The calculations assume a thermo-mechanical calculation scheme. It is assumed that the billet is heated all over its volume to a temperature of 1180°C, and the tool temperature is constant during the whole forming process and it equals 900°C for the piercing plug and 50°C for the rolls and the disc guiding devices. On the basis of the specialist literature [15], it is assumed that the coefficient of the heat exchange between the tools and the metal is of 4000 W/m^{2}K, while the coefficient determining the heat exchange between the metal and the environment is of 200 W/m^{2}K.

TABLE 1

List of parameters for rotary piercing cases assumed in numerical simulation

No.	Feed angle α	Spacing a	Spacing b	Reduction δ	Plug advance c	Plug diameter d_g	Plug length l_g	Plug radius R_g
1.	8°	252.98 mm	335.64 mm	11.7%	35 mm	32 mm	48.9 mm	114.2 mm
2.	8°	252.98 mm	335.64 mm	11.7%	35 mm	34 mm	52.0 mm	118.7 mm
3.	8°	252.98 mm	335.64 mm	11.7%	35 mm	36 mm	55.0 mm	123.0 mm
4.	8°	252.98 mm	335.64 mm	11.7%	32 mm	32 mm	48.9 mm	114.2 mm
5.	8°	252.98 mm	335.64 mm	11.7%	38 mm	32 mm	48.9 mm	114.2 mm
6.	6°	252.98 mm	335.64 mm	11.7%	35 mm	32 mm	48.9 mm	114.2 mm
7.	10°	252.98 mm	335.64 mm	11.7%	35 mm	32 mm	48.9 mm	114.2 mm
8.	8°	251.60 mm	334.18 mm	14.0%	35 mm	32 mm	48.9 mm	114.2 mm
9.	8°	250.40 mm	332.92 mm	16.0%	35 mm	32 mm	48.9 mm	114.2 mm

Owing to the changes in the direction of the friction forces affecting the material-tool contact surface, the calculations assume a constant friction model depending on the metal slipping velocity relative to the tool, which is described with the equation:

$$\tau = -mk \arctan\left(\frac{v_p}{a_p}\right)\frac{v_p}{|v_p|} \tag{2}$$

where m denotes the friction factor, k denotes the pure shear flow stress, v_p denotes the slipping velocity vector, a_p denotes the coefficient several times smaller than the slipping velocity (the calculations assume that a_p equals 0.1% of the roll velocity). Given the lack of lubrication and purposeful roughness of the rolls (to make the billet enter in between the rolls more easily), it is assumed that the friction factor m for the rolls reaches the boundary value of 1.0. The assumed value of the friction factor m for the remaining tools (the discs and the piercing plug) is smaller and it equals 0.7.

Fig. 2 shows one of the developed FEM models of the piercing process. The model consists of two barrel rolls, two disc guiding devices, the piercing plug, and the billet. All the tools were modelled as rigid bodies. To model the billet, eight-noded rectangular elements were used.

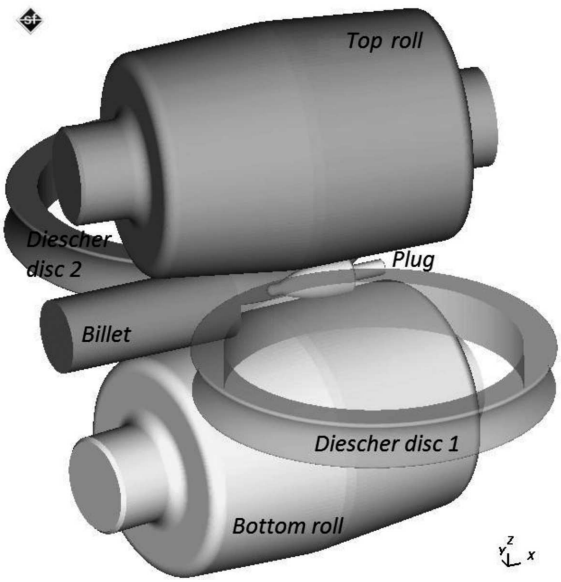

Fig. 2. Model of the rotary piercing process designed with Simufact.Forming 10.0

3. FEM model validation

To validate the developed numerical model, experimental tests of the piercing process were performed using a laboratory rolling mill (Fig. 3) available at the AGH University of Science and Technology in Cracow, Poland. With such mill, it is possible to use different types of working rolls, a different roll assembly (in a two- or three-roll system) as well as different guiding devices (including the disc guides of the Diescher type). The skew mill was equipped with a special meter circuit, which made registering the force parameters possible. The stand was additionally equipped with a heat furnace used to heat the billets.

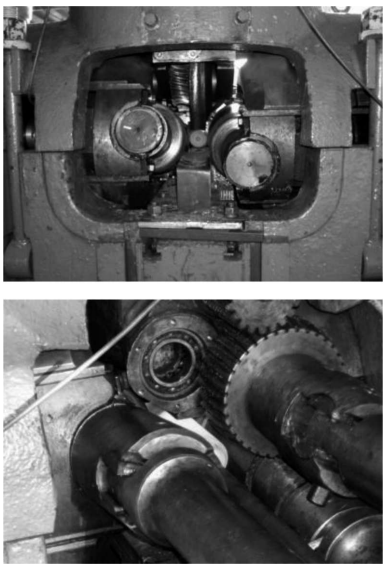

Fig. 3. View of the laboratory skew mill with a two-roll assembly; from the side where the billet is fed (top figure), from the side where thick-walled tube shells are collected (bottom figure)

The experimental rolling tests were performed for three types of piercing plugs at the constant value of the plug advance c equal to 35 mm. Three forming cases were performed and their parameters (the tool and billet dimensions, the material type, the tool velocity, the heating temperature etc.) were identical to the ones assumed in the numerical simulation (Table 1 – items 1, 2 and 3, respectively).

The validation of the developed FEM model of the piercing process consisted in comparing the thickness of the tube blank walls (Fig. 4) and the values of the forces affecting the plug (Fig. 5) which were calculated numerically and measured experimentally. The wall thickness was measured on both ends

of the tube blank. The comparison of the force values concerned the steady state of the piercing process. The analysis of the data shown in Figs. 4 and 5 shows agreement between the numerically calculated parameters and the experimental results, which confirms the validity of the developed FEM model of the piercing process in the skew mill.

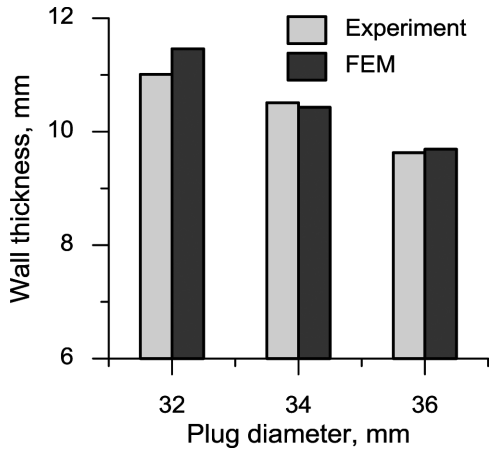

Fig. 4. Comparison of the wall thickness of the tube shells produced in the piercing process at: α =8°, δ =11.7%, c =35 mm

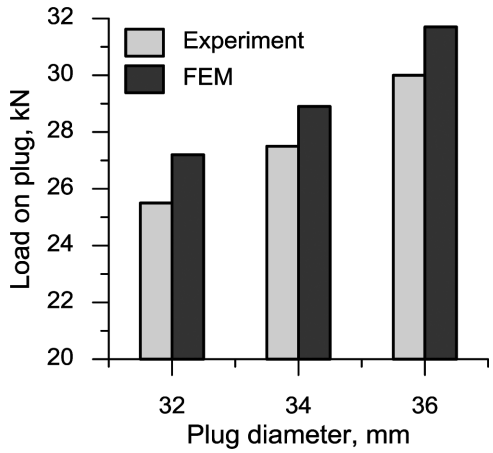

Fig. 5. Comparison of the forces affecting the plug in the steady state of the piercing process at: α =8°, δ =11.7%, c=35 mm

4. Numerical analysis results

The application of the FEM to the analysis of the rotary piercing process allows for investigating the semi-finished product shape changes in the course of rolling. The changes are shown in Fig. 6 in which one of the disc guiding devices is not shown for the purposes of clarity. At the beginning of the process, the billet is gripped by the rolls which make it rotate and move it in the axial direction. It is in this forming stage that the rotary compression process is realized, which continues until the plug nose contacts the frontal surface of the semi-finished product. What begins then is the forming of a tube shell hole whose dimension predominantly depends on the piercing plug used. In the course of forming the tube shell hole, the disc guides also contact the metal; as they rotate, the disc guides increase the axial forces which put the semi-finished product on the piercing plug. Once the plug has completely sunk into the metal, the forming process reaches its steady state which is characterized by a relative stability of the forming forces.

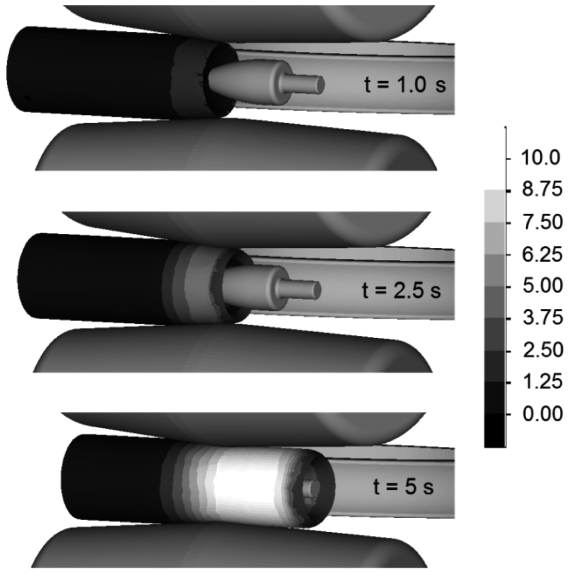

Fig. 6. Semi-finished product shape progression in the rotary piercing process (case no. 1) with the effective strain distribution indicated

In the course of rolling, the object being formed rotates and this rotational motion is the dominant one (Fig. 7). The material reaches the highest linear velocity values on the contact surface with the rolls. It is also there where the friction forces occur which make the object rotate and move it in the axial direction. As a result, the material in the piercing process moves helically. The most intensive axial material flow occurs at the surface area which is adjacent to the rolls, while the least intensive axial material flow occurs in front of the piercing plug nose. The axial material flow is homogenous all over the volume of the formed tube shell (Fig. 8).

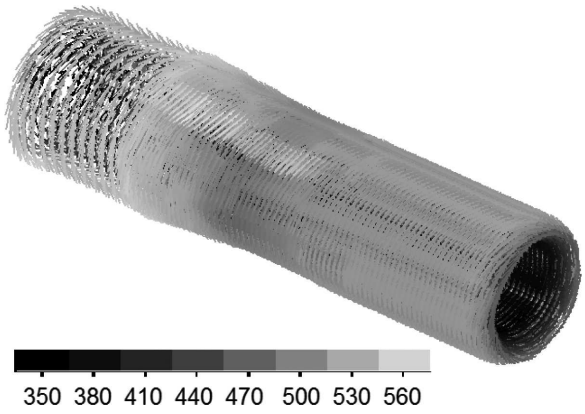

Fig. 7. Distribution of the material flow velocity (in mm/s) in the steady state of the piercing process (case no. 9)

Fig. 9 shows the contact areas with the tools in the steady state of the piercing process. Owing to the impact of the rolls, the material undergoes ovalisation, as a result of which it does not contact the plug all over its perimeter. The cross-sectional ovalisation of the semi-finished tube shell is effectively removed by the disc guides which prevent the material from flowing sideways. Fig. 9 also shows that the contact area between the material and the piercing plug is considerably vast,

as a result of which the heat is intensively carried away to this tool and, consequently, the tool gets heated quickly.

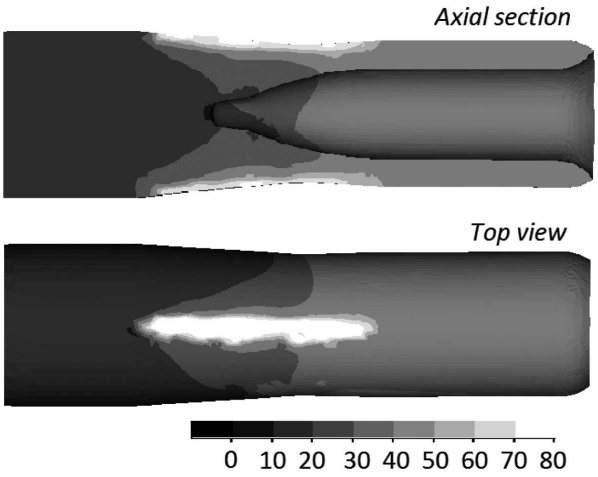

Fig. 8. Distribution of the axial material flow velocity (in mm/s) in the steady state of the piercing process (case no. 9)

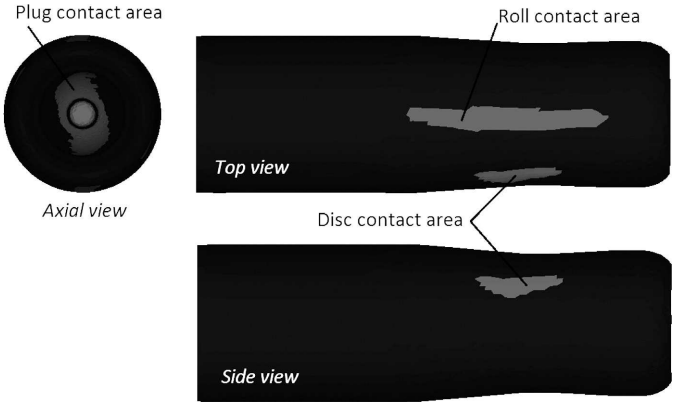

Fig. 9. Contact area between the semi-finished product and the tools in the steady state of the piercing process (case no. 7, t=4 s)

The piercing plug works under the most difficult working conditions. Apart from intensive heating, this tool is subject to high surface stresses (Fig. 10). The highest stresses occur on the piercing plug nose where their values range from 100÷200 MPa. Considerably lower stresses (below 75 MPa) occur in the conical area of the plug; these stresses are found in the roll plane. The determined values of unit pressures are identical to the values given in the specialist literature [1] on forming alloy steels. Again, this proves that the piercing process using the skew mill with the disc guides was modelled correctly.

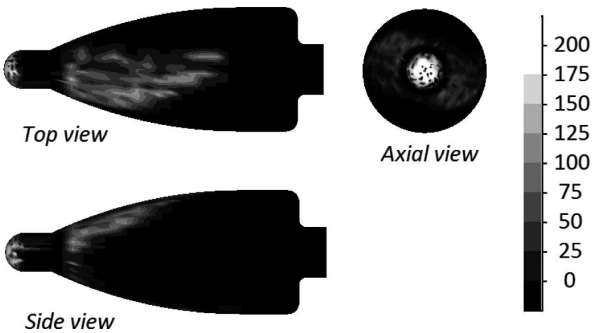

Fig. 10. Distribution of the surface thrusts (in MPa) affecting the plug in the steady state of the piercing process (case no. 8)

Fig. 11 shows the FEM calculated effective strain distributions in the semi-finished products that were formed in the discussed piercing cases. The data show that the biggest strains occur in the tube wall and they can be found near its internal surface. It is worth emphasizing that an increase in the plug diameter does not result in an increase in the maximum values of the effective strain; yet, it contributes to smaller disproportions as for the distribution of this parameter on the tube wall thickness. Analyzing the strain distributions shown in Fig. 11, it can be observed that their values are very high. This results from the metal structure internal shearing which occurs during the forming process; the internal shearing of the metal structure does not result in a desired shape change and causes redundant metal strain. Such redundant metal strain is most intensive on the external surface of the tube shell which is affected by the friction forces mainly responsible for the circumferential (tangential) material flow. The occurrence of considerable redundant strains is characteristic of the skew and cross rolling processes.

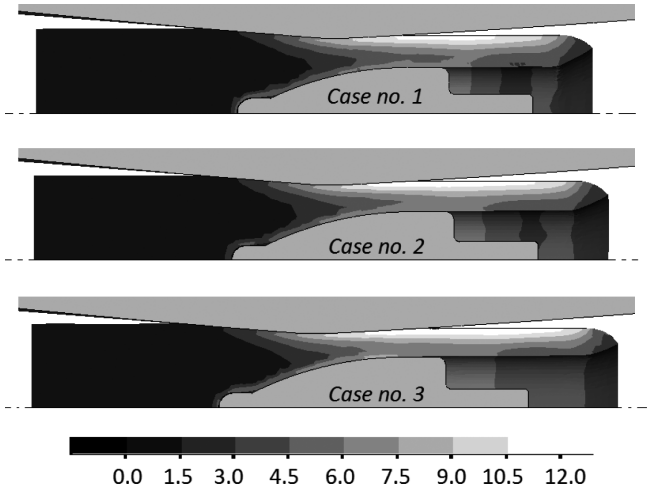

Fig. 11. Effective strain distribution in the semi-finished product obtained in the rotary piercing process (for $t \approx 5$ s)

An analysis of the normal stress distributions shown in Fig. 12 also provides interesting observations. To facilitate the analysis, these stresses are denominated – in accordance with Fig. 2—as axial σ_x, vertical σ_z, and horizontal σ_y. The enumerated normal stresses are shown in two planes: in the roll plane (parallel to the xz plane – Fig. 2) and in the disc plane (parallel to the xy plane – Fig. 2); both of which cross the axis of the product which is being formed. It can be observed that the material is subject to intensive compression due to the impact of the rolls and the piercing plug. The dominant state of the compressing stresses should be considered favourable because the material coherence is retained. At the same time it should be noted that the horizontal stretching stresses σ_y occur in some areas of the product formed. They reach the highest values in the axial area located in front of the piercing plug nose. The vertical compressing stresses σ_z also occur in this area. This means that the stresses which occur in this area change cyclically from the stretching to the compressing ones and vice versa (as the semi-product rotates), which may lead to material cracking in front of the plug, which, in turn, results in a worse quality of the internal surface of the produced thick-walled tube shell. What is more, the horizontal

stretching stresses σ_y occur on the internal surface of the tube (in the roll plane), which results from an increase in the tube hole diameter occurring during the sizing stage of the piercing process (when the tube comes off the plug).

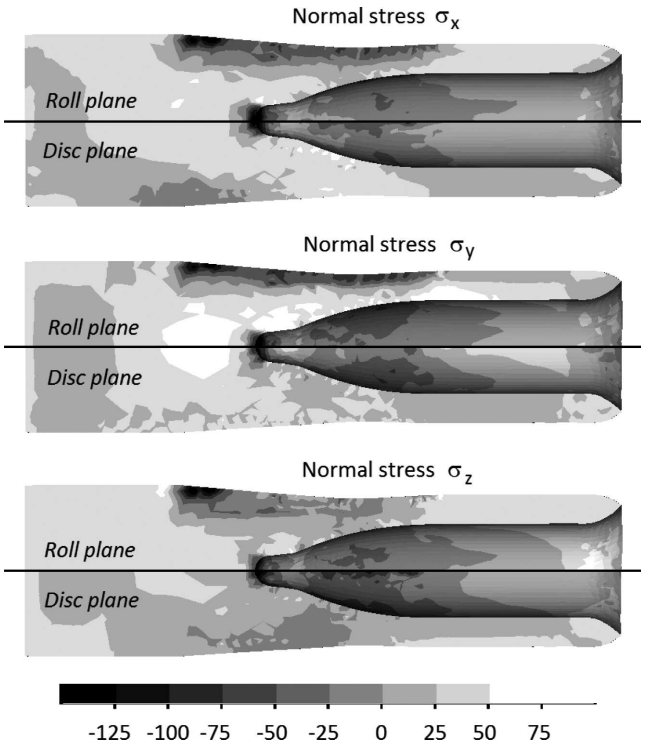

Fig. 12. Normal stress distribution (in MPa) in the semi-finished product determined in the steady state stage of the piercing process (case no. 9)

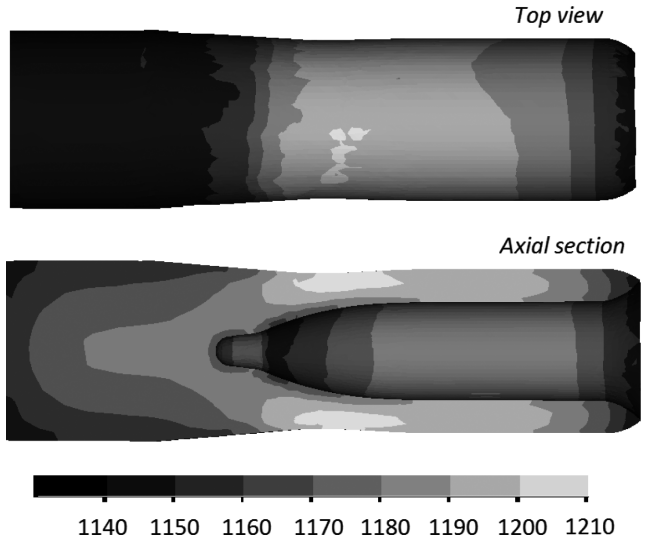

Fig. 13. Temperature distribution (in °C) in the pierced semi-finished product (case no. 8, t=5.2 s)

Fig. 13 shows temperature distributions of the product formed in the piercing process. Despite a relatively long forming time, the metal temperature of the wall of the rolled tube is equal to the billet temperature (1180°C). It is so because the heat generated by the strain work and by the friction work compensates for the losses of the heat carried away to the tools. The lowest temperature values are observed at the ends of the product formed, as it there where the optimal conditions for carrying away of the heat to the environment occur.

The application of the FEM allows for a precise determining of particular tool loads during the piercing stage. Distributions of the forces with which the tools affect the material in one of the analyzed forming cases are shown in Fig. 14; additionally, the figure schematically shows the shape progression of the semi-finished product. It can be noted that all the forces gradually increase their values at the beginning until the moment when the tube shell comes off the piercing plug. After that, the steady state of the process begins in which the force values are maintained on the constant level. It is worth noting that the load of both rolls is practically identical. Some differences can be noticed in the load distributions of particular disc guides, which is a result of uneven clamping pressure of the semi-finished product to the tools. The forces affecting the rolls are two times bigger than the forces which occur on the discs and the piercing plug.

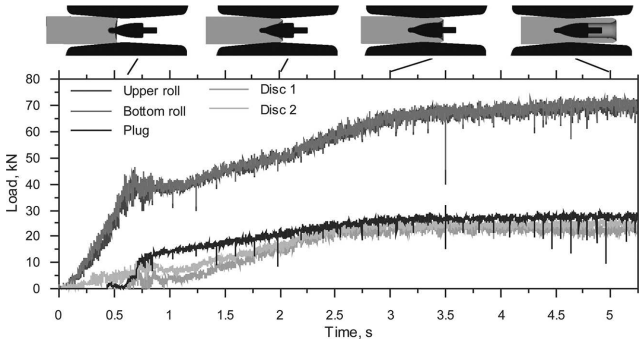

Fig. 14. Distributions of the forces affecting the tools (indicated according to Fig. 2) in the piercing process (case no. 8)

The distribution of the turning moments of the rolls and of the disc guides, which is illustrated in Fig. 15, can be used to determine power demand of the mill. It can be clearly observed that the roll driver plays a decisive role in this respect. The turning moment of the discs is several times smaller, which predominantly results from the position of the resultant force affecting the disc; the force is pointed at a small angle toward the z direction that overlaps with the direction of the disc rotation axis. As for the distribution of the turning moments, it can be stated that it is similar to the force distributions shown in Fig. 14.

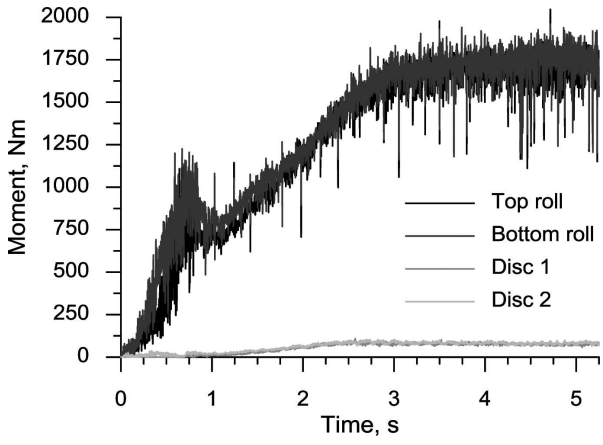

Fig. 15. Distributions of the turning moments affecting the tools (indicated according to Fig. 2) in the piercing process (case No. 8)

The performed FEM simulations allowed for analyzing the effect of particular piercing process parameters on the course of the process. Fig. 16 illustrates the changes in the external and internal diameters (and, consequently, in the wall thickness) of the produced tube shell depending on the plug diameter, the plug advance, the feed angle, and the reduction. It can be clearly observed that it is the diameter of the applied plug that affects the internal diameter most. The effect of the remaining process parameters on this tube shell dimension is negligible. The external diameter, on the other hand, mainly depends on the plug advance and the applied reduction. An increase in the values of these parameters results in a clear decrease in the external diameter.

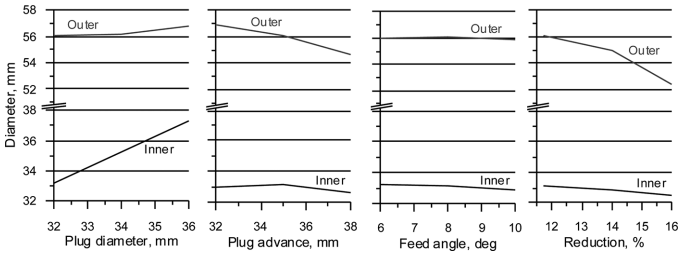

Fig. 16. Effect of the piercing parameters on the diameter dimensions of the tube shells obtained in the piercing process using the Diescher mill

Fig. 17 shows a comparison of the values of the forces affecting particular tools in the analyzed cases of the piercing process. The presented comparison was made by averaging the values of the forces occurring in the steady state of the process. An analysis of the data presented in this figure proves that these are the rolls that are the most loaded in the piercing process, while the disc guides are the least loaded. As far as the effect of the piercing parameters on the force values is concerned, it can be observed that the roll load increases together with an increase in the reduction (which constitutes the decisive parameter) and in the plug diameter, while it decreases to a small extent as the plug advance or the feed angle increase. As for the piercing plug, it can be stated that an increase in this tool load is due to the application of plugs with bigger diameters and the application of bigger feed angles. The forces affecting the disc guides increase their values with increasing the reduction and the piercing plug diameter.

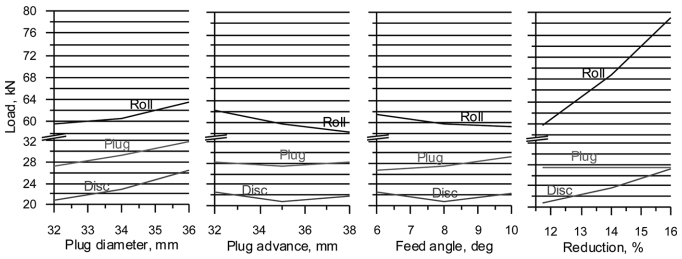

Fig. 17. Effect of the piercing parameters on the tool load in the steady state of the piercing process using the Diescher mill

5. Conclusion

The paper presents a theoretical-experimental analysis aimed at determining the effect of the basic process parameters on the course of the rotary piercing process. The numerical simulations of the piercing process were performed using Simufact.Forming 10.0. Additionally, the analyses of three of the discussed forming cases were conducted in laboratory conditions at the AGH University of Science and Technology in Cracow, Poland. The agreement of the analytical results with the experimental results concerning the tube shell wall thickness and the forces affecting the plug confirms the validity of applying the FEM to analyse such complex forming process as rotary tube piercing. The developed model allows for analyzing the states of stress and strain, the temperature distributions in the formed product as well as the force and energy parameters. The devised FEM model of the piercing process can be further developed to calculate, for example, stresses in the forming tools.

REFERENCES

[1] J. Kazanecki, Production of seamless pipes. Ed. AGH, Krakow 2003 (in Polish).

[2] S. Urbański, J. Kazanecki, Assessment of the strain distribution in the rotary piercing process by the finite element method, Journal Materials Processing Technology **45**, 335-340 (1994).

[3] J. Pietsch, P. Thievien, FEM simulation of the rotary tube piercing process, MPT International **2**, 52-60 (2003).

[4] E. Ceretti, C. Giardini, A. Attanasio, F. Brisotto, G. Capoferri, Rotary tube piercing study by FEM Analysis: 3D simulations and Experimental Results, Tube & Pipe Technology 2004, March/April, 155-159.

[5] K. Komori, Simulation of Mannesmann piercing process by the three-dimensional rigid-plastic finite-element method, International Journal of Mechanical Sciences **7**, 4, 1838-1853 (2005).

[6] Z. Pater, J. Kazanecki, J. Bartnicki, Three dimensional thermo-mechanical simulation of the tube forming process in Diescher's mill, Journal of Materials Processing Technology **177**, 167-170 (2006).

[7] L. Lu, Z. Wang, F. Wang, G. Zhu, X. Zhang, Simulation of Tube Forming Process in Mannesmann Mill, J. Shanghai Jiaotong Univ. (Sci) **16**(3), 281-185 (2011).

[8] Z. Pater, J. Kazanecki, Thermo-mechanical analysis of piercing plug loads in the skew rolling process of thick-walled tube shell, Metallurgy and Foundry Engineering **32**, 31-40 (2006).

[9] K. Komori, K. Mizuno, Study on plastic deformation in cone-type rotary piercing process using model piercing mill for modeling clay, Journal of Materials Processing Technology **209**, 4994-5001 (2009).

[10] A. Ghiotti, S. Fanini, S. Bruschi, P.F. Barianu, Modelling of the Mannesmann effect, CIRP Annals – Manufacturing Technology **58**, 255-258 (2009).

[11] R. Pschera, J. Klarner, Ch. Sommitsch, FEM modeling of cross rolling using damage mechanics. Steel Research International. Special edition "Metal Forming 2008" **1**, 349-356 (2008).

[12] V.P. Romanenko, P.L. Alekseev, E.A. Kharitonov, A.A. Yandimirov, A.A. Sevastyanov, Study on temperature regimes in the heating and piercing of steel ingots to obtain thick-walled shells. Metallurgist **55**, 28-33 (2011).

[13] Z. P a t e r, A. T o f i l, Experimental and theoretical analysis of the cross – wedge rolling process in cold forming conditions. Archives of Metallurgy and Materials **52** (2), 289-297 (2007).

[14] Z. P a t e r, A. G o n t a r z, G. S a m o ł y k, J. B a r t n i c k i, Analysis of cross rolling process of toothed titanium shafts. Archives of Metallurgy and Materials **54** (3), 617-626 (2009).

[15] J.C. P r i n c e, R. M a r o n o, F. L e o n, Thermomechanical analysis of a piercing mandrel for the production of seamless steel tubes. Proceedings of the Institution of Mechanical Engineers, Part E: Journal of Process Mechanical Engineering **217**, 337-34 (2003).

Received: 20 March 2012.